

Electrochemical and Theoretical Evaluation of 5,5'-(Pyridine-2,6-diyl)bis(4-phenyl-4H-1,2,4-triazole-3-thiol) as a Novel Corrosion Inhibitor of Mild Steel in the Acidic Medium

Majid Khodaei-Tehrani*, Ali Niazi

Department of Chemistry, Arak branch, Islamic Azad University, Arak, Iran

*E-mail: m.khodaei.tehrani@gmail.com; m-khodaei92@iau-arak.ac.ir

Received: 13 January 2015 / Accepted: 20 March 2015 / Published: 24 June 2015

The inhibition properties of 5,5'-(Pyridine-2,6-diyl)bis(4-phenyl-4H-1,2,4-triazole-3-thiol) (PDPTT) on corrosion of mild steel in acidic media (1 M HCl) were analyzed by weight loss measurements and electrochemical techniques. The PDPTT exhibits good inhibition properties in hydrochloric acidic solution and the calculated values of $\Delta G_{\text{ads}}^{\circ}$ revealed that the adsorption mechanism of PDPTT on steel surface is due to between chemi- and physisorption. The adsorption of PDPTT on the steel surface, in 1 M HCl solution, obeys to Langmuir's isotherm. Quantum chemical calculation functions were applied to correlate electronic structure parameters of PDPTT with their inhibition performances. The reactive sites predicted by condensed Fukui functions during electrophilic and nucleophilic attacks are successfully revealed.

Keywords: Corrosion, Inhibitor, Mild steel, Electrochemical techniques, Polarization, Theoretical study.

1. INTRODUCTION

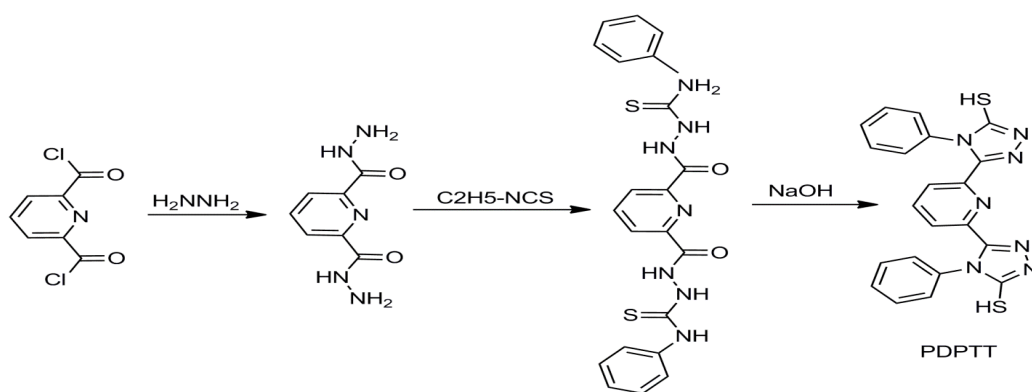
There are various purposes to apply acid solutions greatly in industry, for example acid pickling, unfavorable scale removal, and boilers as well as heat exchangers cleaning. Corrosion inhibitors are considered as a significant procedure for metallic materials protection against corrosion in acidic medium [1, 2]. The corrosion inhibitors that are effective include organic compounds, like N, O, S atoms. The nature and condition of the metallic surface, the chemical composition and structure of the inhibitor are the factors that make the organic inhibitors effective. A better inhibition performance depends on the inhibitors having N and S simultaneously [3, 4]. Molecular structure, electron density at their donor atoms, hydrophobicity, solubility and dispersibility are considered as the

most significant factors playing a role in choosing an inhibitor [5]. A great number of authors have conducted research on the effect of organic compounds that include nitrogen and sulfur [6, 7]. Chemicals such as triazoles which are acceptable environmentally are regarded among different nitrogenous compounds as inhibitors. A great number of replaced triazole and pyridine compounds as effective corrosion inhibitors have been studied profoundly for steel in acidic media [8-10]. In order to assess the inhibition performance of corrosion inhibitor, Quantum chemistry calculation is applied in a wide manner. The prediction of donation or acceptance of electrons by capable inhibitor molecules through this method is done by analyzing global reactivity parameters, including energy gap between HOMO and LUMO, chemical potential, etc. By analyzing interfacial configuration, interaction between inhibitor and metal surface, etc., the adsorption state of inhibitor on metal surface can be studied [11, 12]. Determining the efficiency of corrosion inhibition, 5,5'-(Pyridine-2,6-diyl)bis(4-phenyl-4H-1,2,4-triazole-3-thiol) (PDPTT) as novel inhibitor for the corrosion of carbon steel in 1.0 M HCl is considered as the purpose of this study. By means of three various methods, including electrochemical impedance spectroscopy (EIS), potentiodynamic polarization and weight loss measurements, it was possible to determine the efficiency of inhibition. On the basis of the B3LYP Density Functional Theory (DFT) method, the quantum theoretical calculations were carried out in order that the electronic properties of the studied inhibitor are clarified.

In this molecule class, it was understood that the conclusions of theoretical calculations were consistent with the experimental results.

2. EXPERIMENTAL

2.1. Synthesize of symmetrical pyridine derivatives



Scheme 1. Synthetic pathway for preparation of PDPTT.

Synthesis of The 5,5'-(Pyridine-2,6-diyl)bis(4-phenyl-4H-1,2,4-triazole-3-thiol) (PDPTT) were made through multistep reaction sequences and prior to its application, it was characterized via IR spectroscopy, ^1H NMR, ^{13}C NMR spectroscopy and element analysis [13]. Scheme 1 indicates the

synthetic route of how to prepare these compounds. In addition, Figure 1 shows molecular structure as well as atom numbering of the studied inhibitor.

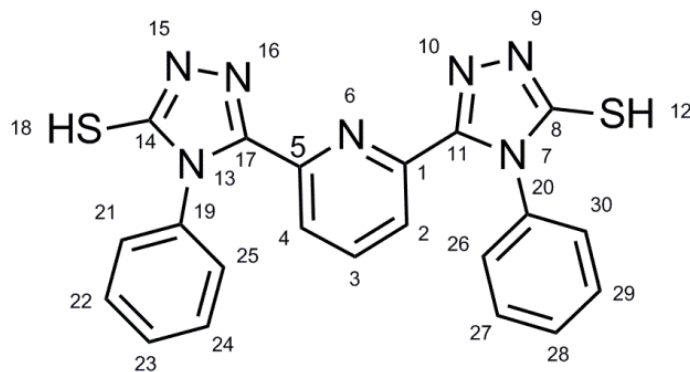


Figure 1. Molecular structure and atom numbering of investigated inhibitor.

2.2. Materials

The whole experiments with the chemical composition (in wt.%) such as 0.412% C, 0.256% Si, 0.615% Mn, 0.0249% S, 0.0165% P, 0.368% Cr, 0.0458% Mo, 0.159% Ni, 0.139% Cu, were carried out on mild steel and the rest of the iron was applied to the electrochemical studies. Irrespective of the bottom surface of the working electrode with a surface area of 1 cm², its coating was made of polyester. Prior to each experiment, samples were ground down to 1200 grit abrasive SiC paper from the mechanical point of view; put into deionized water for washing and then exposed to hot air for drying. Preparation of the solutions (1 mol L⁻¹ HCl) was made through an analytical reagent grade 37% HCl diluted with water that is distilled doubly. By means of a thermostat-cooling condenser, the experiments were conducted at miscellaneous temperatures (with ± 1 °C accuracy).

2.3. Electrochemical measurements

Applying an AUTOLAB model PGSTAT12 (Eco Chemie, Utrecht and The Netherlands) and in a three-electrode electrochemical cell, polarization and impedance were studied. In a conventional three-electrode cell configuration, electrochemical measurements were done in which mild steel was determined as working electrode, saturated calomel electrode (SCE) as reference electrode, and a platinum wire was used as an auxiliary electrode. A report was made for all potentials vs. SCE. The electrode was put inside a test solution at open circuit potential (OCP) for an hour prior to any measurement. Linear polarization resistance (LPR) test was completed using constant sweep rate (0.5 mV s⁻¹) with scanning differing from -150 to +150 mV around OCP. Analysis of polarization data was performed by means of GPES electrochemical software. Electrochemical impedance spectroscopy (EIS) was measured in a frequency range of 10 kHz to 0.01 Hz with amplitude of 10 mV peak-to-peak by means of AC signals at OCP. Analysis of impedance data are done by FRA software.

2.4. Weight loss measurements

In a double walled glass cell with a thermostat-cooling condenser, weight loss measurements were conducted. Weighing the cleaned steel samples prior to and after putting into 80 ml of 1.0 mol L⁻¹ HCl solution with and without different concentrations of PDPTT, weight loss designated at different immersion times at 30 °C. With and without 0.004 mol L⁻¹ inhibitor after 8 h of immersion time the tests were carried out repeatedly at various temperatures from 30 to 60 °C. The weight loss measurements were performed in triplicate and the average weight loss was recorded.

Calculation of the corrosion rate (W) was conducted from the weight loss values, from the equation [14] as follows:

$$W = \frac{\Delta m}{St} \quad (1)$$

Where Δm is considered as the mass loss in (mg), S as the area of the mild steel coupon (cm²), t as the immersion period in (h) and W as the corrosion rate in (mg cm⁻² h⁻¹).

Applying the equations (1) and (2) [15], the calculation of the surface coverage (θ) and inhibition efficiency (IE%) of each concentration was done:

$$\theta = \frac{W_{corr}^0 - W_{corr}}{W_{corr}^0} \quad (2)$$

$$IE\% = \frac{W_{corr}^0 - W_{corr}}{W_{corr}^0} \times 100 \quad (3)$$

Where W_{corr}^0 and W_{corr} are considered as the values of corrosion rates of mild steel samples in the absence and presence of inhibitors in a respective manner.

2.5. Quantum chemical study

Using DFT (density functional theory) with The Becke's three-parameter hybrid functional, the structures were improved by the Lee, Yang, and Parr (LYP) correlation functional [16]; denoted as B3LYP theory, and used in the DFT calculations by means of 6-31G (d,p) basis set. The quantum chemical calculations were carried out with complete geometry. Optimizations are done using Gaussian 03 (Review B.05) program software package [17]. The adsorption centers of the inhibitors can be predicted based on Koopman's theorem [18], Frontier molecular orbitals (HOMO and LUMO). Adsorption should happen at the part of the molecule in which the softness, σ , as the local property, has the highest value in order to simplify transfer of electrons. The E_{HOMO} and E_{LUMO} of the inhibitor molecule are concerned with the electron affinity, A, and the ionization potential, I, respectively, are given by:

$$I = -E_{HOMO} \quad (4)$$

$$A = -E_{LUMO} \quad (5)$$

Calculation of absolute electronegativity, χ , and absolute hardness, η , of the Inhibitor molecule were conducted applying the values of I and A and given by:

$$\chi = \frac{I + A}{2} \quad (6)$$

$$\eta = \frac{I - A}{2} \quad (7)$$

And the global softness, σ , is the inverse of the global hardness:

$$\sigma = \frac{1}{\eta} \quad (8)$$

Thus the fraction of electrons transferred from the inhibitor to metallic surface, ΔN , as follows [19]:

$$\Delta N = \frac{\chi_{Fe} - \chi_{inh}}{2(\eta_{Fe} + \eta_{inh})} \quad (9)$$

3. RESULTS AND DISCUSSION

3.1. Weight-loss measurements

Due to its reliability and simple application [20], the weight loss method is beneficial and it is applied to control corrosion rate. Weight loss of mild steel was performed in 1 mol L⁻¹ HCl after immersing for 8 hours with or without different concentrations of PDPTT. In Table 1, the calculated values of corrosion rate and inhibition efficiency are indicated by means of equations (1) and (3), in a respective manner. In Table one, the corrosion rate variation (W) is indicated with inhibitor concentrations. According to the results, the corrosion inhibition efficiencies for PDPTT increase with increasing inhibitor concentration.

Table 1. Weight loss results of mild steel corrosion in 1.0 mol L⁻¹ HCl with addition of various concentrations of inhibitors at 30 °C.

Inhibitor	C _{inh} (molL ⁻¹)	W (mg cm ⁻² h ⁻¹)	Θ	IE (%)
	Blank	1.338	-	-
PDPTT	0.00025	0.366	0.726	72.6
	0.0005	0.324	0.758	75.8
	0.001	0.278	0.792	79.2
	0.002	0.222	0.834	83.4
	0.004	0.135	0.899	89.9

3.2. Potentiodynamic polarization

In Figure 2, the polarization behavior of carbon steel in 1.0 mol L⁻¹ HCl with and without different concentrations of synthesized inhibitors is shown at 30 °C. Calculations of the corrosion current density values (I_{corr}), corrosion potential (E_{corr}), cathodic Tafel slope (β_c), and anodic Tafel slope (β_a) as functions of synthesized inhibitor concentration were performed from the curves in Figure 2 and listed in Table 2. The I_{corr} values were applied to calculate the inhibition efficiency, IE (%) (Table2) using the equation [21] as follows:

$$IE\% = \left[1 - \frac{I_{corr}}{I_{corr}^0} \right] \times 100 \quad (10)$$

Where I_{corr} and I_{corr}^0 were known as the inhibited and uninhibited corrosion current densities in a respective manner and determined by extrapolation of the cathodic and anodic Tafel lines to the corresponding corrosion potentials. Both the anodic metal dissolution and cathodic hydrogen evolution reactions were inhibited after inhibitors were added to the aggressive medium based on Figure 2. The existing synthesized inhibitors changed the corrosion potential (E_{corr}) slightly to positive direction and did not change in the inhibited solution greatly in comparison to the uninhibited solution and, it denotes that the synthesized inhibitors acted as mixed type inhibitor [22, 23]. In Figure 2, the net cathodic current density with inhibitors is indicated nearly independent of inhibitor concentration even though the net anodic current density decreases by adding the inhibitor concentration.

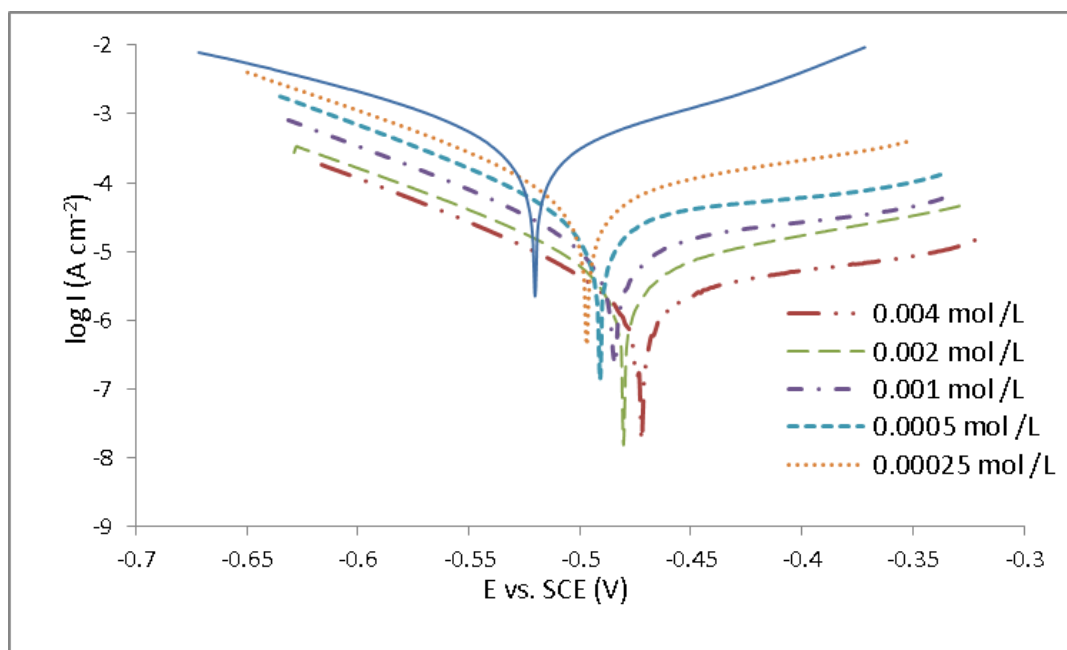


Figure 2. Potentiodynamic polarization behavior of mild steel in 1 mol L⁻¹ HCl without and with the addition of different concentrations of PDPTT at 30 °C.

An increase in inhibitor concentration tends to block more anodic sites, which are appropriate for metal dissolution. Adsorption of organic inhibitor molecules onto a metal surface and hence retarding the metal dissolution and, as a consequence, hydrogen evolution by blocking available sites is widely accepted by other researchers [24, 25]. The variation of β_C values with changes in the concentration of inhibitor indicates the influence of compounds on the kinetics of hydrogen evolution. Also, the shift in the anodic tafel slope (β_a) may be inhibitor modules adsorbed onto the steel surface /or due to the chloride ions [26].

Table 2. Potentiodynamic polarization parameters obtained by Tafel polarization technique for mild steel in various concentrations of the synthesized inhibitors of 1.0 mol L⁻¹ HCl at 30 °C.

Inhibitor	C _{inh} (M)	E _{corr} vs SCE (mV)	I _{corr} (mA cm ⁻²)	β _a (mV dec ⁻¹)	β _C (mV dec ⁻¹)	IE%
	Blank	522	297	86	126	-
PDPTT	0.00025	499	64.75	118	128	78.2
	0.0005	493	54.35	132	138	81.7
	0.001	490	46.63	123	132	84.3
	0.002	486	39.50	144	127	86.7
	0.004	482	25.84	112	98	91.3

3.3. Electrochemical impedance spectroscopy (EIS) measurements

In Figure 3, typical Nyquist plots for MS in 1 mol L⁻¹ HCL at 30 °C are indicated with and without the studied inhibitors at various concentrations. One single depressed semicircle is shown by the impedance spectra, and the diameter of semicircle increases with an increase in inhibitor concentration. The charge transfer occurs at electrode/solution interface as the single semicircle indicates; corrosion reaction of metal is controlled by the transfer process, and the presence of inhibitor does not change the mechanism of steel dissolution [27, 28]. Analysis of the impedance spectra for the Nyquist plots is done by means of the equivalent circuit model shown in Fig. 4. The circuit consists of a constant phase element CPE, parallel to a resistor R_p.

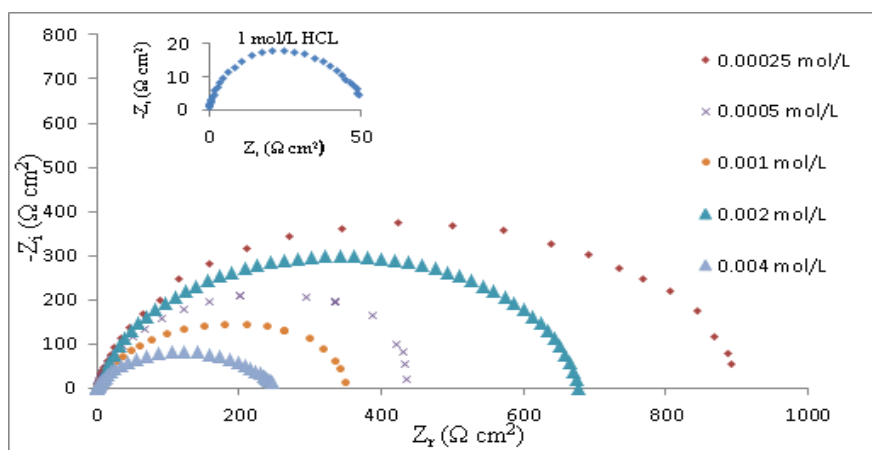


Figure 3. Nyquist plots of mild steel in 1mol L⁻¹ HCl with different concentrations of PDPTT.

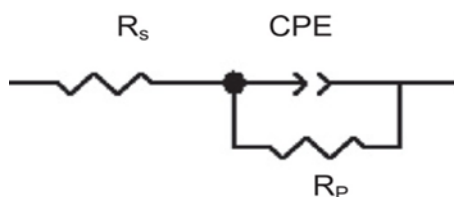


Figure 4. Electrical equivalent circuit used to fit the EIS data of the interface mild steel 1 mol L⁻¹ HCl solution without and with synthesized inhibitor.

The ohmic resistance of the corrosion product films and the solution enclosed between the reference electrode and the working, R_s is indicated by the intersection of the capacitive loop with the real axis. The diameter of Nyquist's plot is consistent with R_p [29]. Calculation of the percentage inhibition efficiency of the inhibitor was carried out from the value of R_p by means of the equation as follows:

$$E\% = \frac{R_{p(inh)} - R_p}{R_{p(inh)}} \times 100 \tag{11}$$

Where R_p and $R_{p(inh)}$ are resistance with or without inhibitor [30]. Therefore, the capacitance is presented by a constant phase element (CPE) determined in impedance representation as [19]:

$$Z_{CPE} = [Q(j\omega)^n]^{-1} \tag{12}$$

Where, Z_{CPE} is considered as the impedance of CPE, Q as the magnitude of CPE, ω as the angular frequency (in rad s^{-1}), j as the imaginary number and n as a CPE exponent, applied as a gauge of the heterogeneity or roughness of the surface [31]. The CPE, which is supposedly a surface irregularity of the electrode, reasons a greater depression in Nyquist semicircle diagram, where the metal–solution interface works as a capacitor with an irregular surface. If the electrode surface is homogeneous, the exponential value (n) is equal to 1 and the metal–solution interface works as a capacitor with a regular surface [32]. Calculation of the double layer capacitance (C_{dl}) was performed by the equation as follow [33]:

$$C_{dl} = \frac{1}{\omega_{max} R_p} \tag{13}$$

Where, ω_{max} is considered as the frequency at maximum imaginary component of the impedance. In Table 3, the percentage inhibition efficiencies, R_s , R_p , C_{dl} and n are shown.

Table 3. Electrochemical impedance spectroscopy parameters of carbon steel electrode in aqueous 1.0 mol L⁻¹HCl solution with and without various concentrations of the synthesized inhibitors at 30 °C.

Inhibitor	C_{inh} (molL ⁻¹)	R_s (Ω cm ²)	R_p	n	C_{dl} (μ F cm ⁻²)	IE (%)
Blank	-	1.53	51	0.843	510	-
PDPTT	0.00025	0.85	270	0.855	474	81.1
	0.0005	0.72	357	0.867	463	85.7
	0.001	0.64	478	0.868	461	85.5
	0.002	0.83	683	0.871	458	87.7
	0.004	0.38	922	0.873	448	94.5

The decrease in C_{dl} is probably because of a decrease in local dielectric constant and/or an increase in the thickness of the protective layer formed at the electrode surface [34]. Based on Helmholtz model, double layer capacitance is inversely proportional to the surface film thickness [35].

$$C_{dl} = \frac{\varepsilon^\circ A}{d} \quad (14)$$

Where, ε is considered as the dielectric constant of the medium, ε° as the vacuum permittivity, A as the electrode surface area, and d as the thickness of the protective layer. The R_p and $IE\%$ values, obtained from the EIS measurements, can be compared and are parallel to those values obtained from the polarization measurements and weight loss measurements.

3.4. Adsorption isotherm

Any information on the metal–inhibitor interaction is presented by the adsorption isotherm. More information can be supplied by the type of the adsorption isotherm about the properties of the inhibitors. Several adsorption isotherms were determined, and the Langmuir adsorption isotherm was found to explain about the adsorption behavior of the investigated inhibitor. The Langmuir isotherm is given by the equation as determined elsewhere [36].

$$\frac{C_{inh}}{\theta} = \frac{1}{K_{ads}} + C_{inh} \quad (15)$$

Calculation of the adsorption free energy (ΔG_{ads}°) was conducted by:

$$K_{ads} = \frac{1}{55.5} \exp\left(-\frac{\Delta G_{ads}^\circ}{RT}\right) \quad (16)$$

Calculation of the adsorption equilibrium constant, K_{ads} was carried out from the intercepts of the straight lines C_{inh}/θ axis. The surface coverage, θ ($\theta = \eta/100$) can be estimated from polarization and impedance results [37]. In Figure 5, the plot of C_{inh}/θ versus C_{inh} yields a straight line is shown with nearly a unit slope.

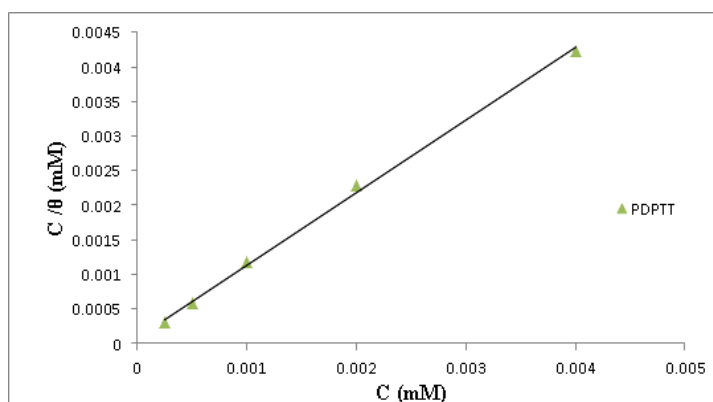


Figure 5. Langmuir adsorption isotherm of inhibitor in 1 mol L⁻¹ HCl at 30 °C.

In Table 5, the thermodynamics parameters derived from Langmuir adsorption isotherms for the studied compounds. The negative values of ΔG_{ads}° along with the high K_{ads} show a spontaneous adsorption process. The values of ΔG_{ads}° up to -20 kJ/mol are attributed to the electrostatic interaction between the charged molecules and the charged metal (physisorption). Hence, those around -40 kJ/mol

or smaller include charge sharing or transfer from organic molecules to the metal surface so as to form a coordinate type of bond (chemisorption). The value of -40 kJ/mol is usually adopted as a threshold value between chemi- and physisorption. Under studied experimental circumstances, the values of $\Delta G_{\text{ads}}^{\circ}$ for these inhibitors refer to the spontaneity of the adsorption process, and it also indicates the adsorption of compounds happening predominantly by chemisorption.

Table 5. Thermodynamic parameters for the adsorption of inhibitor in 1.0 mol L^{-1} HCl on the mild steel at $30 \text{ }^{\circ}\text{C}$.

Inhibitor	R^2	$\Delta G_{\text{ads}}^{\circ}$ (KJ mol $^{-1}$)	K_{ads} (M $^{-1}$)
PDPTT	0.998	-33.61	1.1×10^4

3.5. Effect of temperature

After about eight hours of immersion, weight loss were measured at various temperatures (from 30 to $60 \text{ }^{\circ}\text{C}$) with and without 0.004 M inhibitors and a list of the obtained data is available in Table 6.

Table 6. Effect of temperature on the corrosion rate of mild steel in 1.0 mol L^{-1} HCl and 0.004 mol L^{-1} of inhibitor at 8 hour.

Inhibitor	Temperature				
	30°C	40°C	50°C	60°C	
Blank	W^0 (mg cm $^{-2}$ h $^{-1}$)	1.338	2.093	3.018	3.82
	W (mg cm $^{-2}$ h $^{-1}$)	0.135	0.223	0.327	0.498
PDPTT	%IE	89.9	88.6	87.4	84.6

With an increase in temperature in the inhibited solution, the obtained corrosion rates increases. The Arrhenius equation expresses the dependence of the corrosion rate on temperature. The Arrhenius equation could be written using Equation (17) [38] as follows:

$$\ln(W_{\text{corr}}) = \ln A - \frac{E_a}{RT} \quad (17)$$

Where, W_{corr} is considered as the corrosion rate, A as the Arrhenius pre-exponential factor, R as the gas constant, E_a , as the activation corrosion energy for the corrosion process and indication of adsorption mechanism, will be obtained; and T is known as the absolute temperature. Calculation of the apparent activation energies (E_a) and pre-exponential factors (A) at 0.004 M inhibitor are conducted by linear regression between $\ln W_{\text{corr}}$ and $10^3/T$ (Fig. 6).

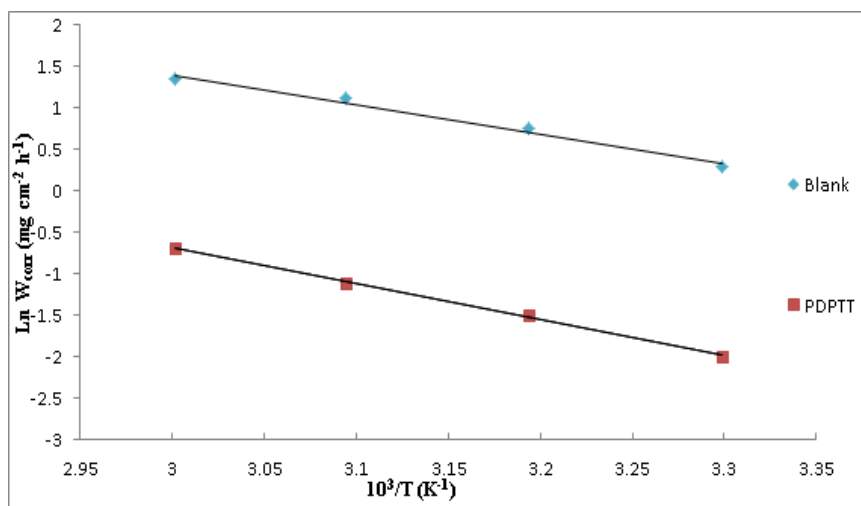


Figure 6. Arrhenius plots of $\ln W_{\text{corr}}$ versus $10^3/T$ with and without 0.004 mol L^{-1} of inhibitor.

E_a values concerning mild steel in $1 \text{ mol L}^{-1}\text{HCl}$ solution with and without the inhibitor are available in Table 7. It can be found out that the higher E_a and the increase in the energy barrier of corrosion reaction with inhibitors may be attributed to the change in the mechanism of the steel dissolution in the presence of adsorbed inhibitor molecule. It is often interpreted by physical adsorption resulting in the formation of an adsorptive film of electrostatic character [39]. Calculation of the values of standard enthalpy of activation (ΔH^*) and standard entropy of activation (ΔS^*) were performed by the equation as follows:

$$W = \frac{RT}{N_A h} \exp\left(\frac{\Delta S^*}{R}\right) \exp\left(-\frac{\Delta H^*}{RT}\right) \quad (18)$$

Where W is considered as the corrosion rate from weight loss measurements, N_A as Avogadro’s number, R as the universal gas constant, and h as Planck’s constant. Plotting of $\ln (W/T)$ against $1/T$, (Eq. (18)), for carbon steel dissolution in $1.0 \text{ mol L}^{-1}\text{HCl}$ with and without 0.004 mol L^{-1} from the synthesized inhibitor, gives straight lines as indicated in Figure 7. Data in Table 7 shows the values ΔH^* and ΔS^* , calculated from the slope of $\Delta H^*/R$ and the intercept of $\ln(R/N_A h) + \Delta S^*$ of the straight line. The data inspection indicates that the activation parameters ΔH^* and ΔS^* of the dissolution reaction of carbon steel in $1.0 \text{ mol L}^{-1} \text{HCl}$ with the inhibitor are higher than those without the inhibitor (blank). Based on the positive signs of ΔH^* reflect, the transition state of the mild steel dissolution is an endothermic process [40]. Based on negative values of signs ΔS^* , an increase in the value of ΔS^* decreases slowly with inhibitors synthesized with inhibition efficiency denoting that the activated complex in the rate designation step shows an association rather than a dissociation step. This means that a decrease in disordering accomplished on going from reactant to the activated complex[41].

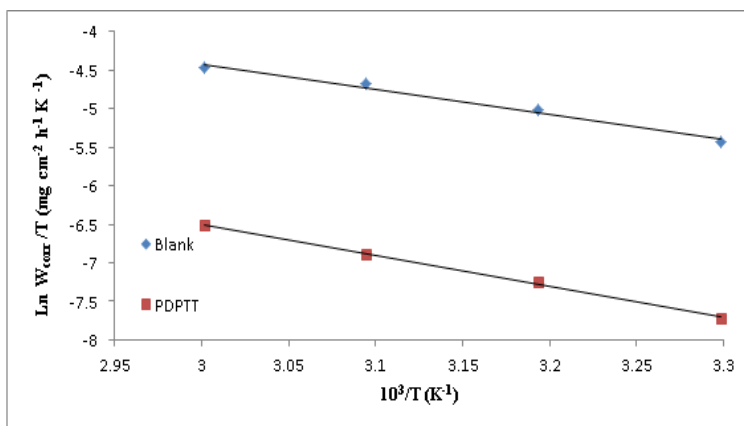


Figure 7. Arrhenius plots of ln (W/T) versus 103/T in the absence and presence of 0.004 mol L⁻¹ of inhibitor.

Table 7. Activation parameters, Ea, ΔH* and ΔS* of the dissolution of mild steel in 1.0 mol L⁻¹ HCl and in the absence and presence of inhibitors.

Inhibitor	K (mg cm ² h)	R ²	Ea (kJ/mol)	ΔH* (kJ/mol)	ΔS* (kJ/mol)
Blank	17.45×10 ⁴	0.989	29.59	26.95	-155.30
PDPTT	22.91×10 ⁴	0.993	36.11	33.48	-150.79

3.6. Quantum chemical study

To do research on the effect of geometric and electronic structural parameters on the inhibition efficiency of inhibitors, quantum chemical calculations were conducted. These studies are considered as powerful tools for studying their adsorption mechanisms about the metal surface [42].

In Figure 8, the improved molecular structures with minimum energies from the calculations are available. In Table 8, there are quantum chemical parameters from the calculations by means of DFT/B3LYP/6-31G (d,p) which are responsible for the inhibition efficiency of inhibitor, such as the energies of highest occupied molecular orbital (E_{HOMO}), energy of lowest unoccupied molecular orbital (E_{LUMO}), the separation energy (E_{LUMO}-E_{HOMO}), ΔE, dipole moment, μ, for the neutral inhibitors. Based on the quantum chemical method, the number of transferred electrons (ΔN) was also calculated as in Equation (9).

In accordance to Pearson’s electronegativity scale and η value of 0 eV/mol for iron atom, the ΔN values showed inhibition effect resulting from electrons donation applying a theoretical χ value of 7 eV/mol. With an increase in electron-donating ability to the metal surface, the inhibition efficiency increases in case ΔN < 3.6. Hence, this inhibitor with low ΔN has the ability to donate good electron to the metal surface.

There is an expectation that the synthesized inhibitor is known as the electron donor, and the steel surface is considered as the acceptor; so this results in chemical adsorption of the inhibitor on the electrode surface. Here, the inhibitor is connected to the steel surface and forms a layer of adsorption against corrosion. The synthesized inhibitor exhibits the highest inhibition efficiency since it has the

capability to produce the highest HOMO energy; therefore, this displays the greatest ability (the lowest ELUMO) to offer electrons. In Table 8, it is observed that the synthesized inhibitor is able to donate electrons to the metal surface, which is in good consistency with the higher inhibition efficiency of the synthesized inhibitor.

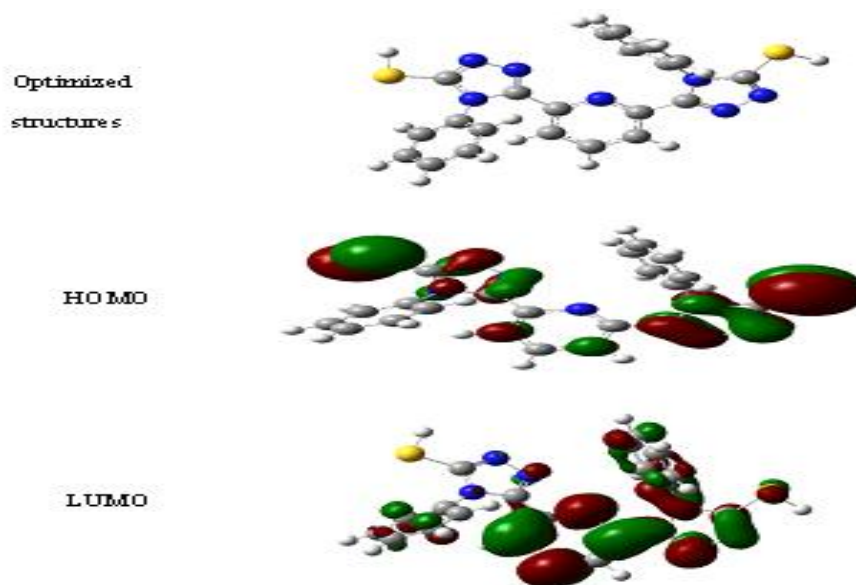


Figure 8. The optimized molecular structure, HOMO and LUMO of the neutral inhibitor molecule by means of DFT/B3LYP/6-31G (d,p).

Table 8. calculated quantum chemical parameters for the neutral inhibitors.

	E_{HOMO} (eV)	E_{LUMO} (eV)	ΔE (eV)	η (eV)	σ (eV ⁻¹)	χ (eV)	μ (D)	ΔN (e)
PDPTT	-5.941	-1.384	4.557	2.278	0.439	3.663	7.032	0.732

3.7. Local Reactivity

Parr and Yang [43] proposed Fukui functions as measurement of local reactivity of the molecules showing the reactive regions and the nucleophilic as well as electrophilic behavior of the molecule. As defined, the Fukui function f_k is the first derivative of the electronic density regarding the number of electrons N in a constant external potential [44]:

$$f_k = \left(\frac{\partial \rho(\vec{r})}{\partial N} \right)_{v(\vec{r})} \tag{19}$$

According to Yang and Mortier [45], Fukui functions can be written as follows:

$$f_k^+ = q_k(N + 1) - q_k(N) \quad (\text{for nucleophilic attack}) \tag{20}$$

$$f_k^- = q_k(N) - q_k(N-1) \quad (\text{for electrophilic attack}) \quad (21)$$

Where $q_k(N)$, $q_k(N+1)$ and $q_k(N-1)$ considered as the atomic charges of the neutral, anionic and cationic species, in the respective manner.

Table 9. The condensed Fukui functions on the atoms of the studied compounds.

Atom	f^-	f^+	$q_k(N)$	$q_k(N+1)$	$q_k(N-1)$
N6	0.075	0.191	-0.553	-0.362	-0.628
N7	0.029	0.003	-0.572	-0.569	-0.601
N9	0.004	0.051	-0.366	-0.315	-0.37
N10	0.026	0.066	-0.314	-0.248	-0.34
N13	0.043	-0.097	-0.558	-0.655	-0.601
N15	0.113	0.024	-0.315	-0.291	-0.428
N16	-0.008	0.08	-0.345	-0.265	-0.337
S12	0.046	0.152	0.047	0.199	0.001
S18	0.074	0.121	0.041	0.162	-0.033

The changes are measured by the f_k^+ in density when the molecule obtains electrons, and it corresponds to reactivity with regard to nucleophilic attack. The nucleophilic attack site will be the place where the maximum value of f_k^+ is observed. On the other hand, the electrophilic attack site is under the control of the f_k^- value, and the highest value of f_k^- corresponds to a possible site for an electrophilic attack.

In Table 4, the Fukui functions values for a nucleophilic and electrophilic attack are available for PDPTT (only for the nitrogen, sulfur atoms). Inspection of the values of Fukui functions in table 4 indicates that PDPTT has propitious zones for nucleophilic attack located on N6, N7, N9, N10, N15, N16, S12, S18 and propitious zones for electrophilic attack located on N6, N7, N9, N10, N13, N15, S12, S18. Data in table 4 shows that PDPTT has a lot of sites that are susceptible to adsorption on the metal surface reflecting the highest inhibition performance. Moreover, the important structural characteristics include the planarity (π) and lone pair of electrons present on the N and S atoms specifying these molecules adsorption to the metal surface. It should be noted that the presence of the C=S group linkage in the organic structure forms $d\pi - d\pi$ bond, resulting from the overlap of 3d electrons from Fe atom to the 3d vacant orbital of the sulfur atom, and thus PDPTT on the metal surface is adsorbed greatly. Also, it is believed that there is good inhibition efficiency of PDPTT since interaction between the π -electrons in the aromatic ring of the PDPTT and the vacant d-orbitals of metal surface. In addition, it is found that the triazole-type compounds consist of many heterocyclic structures making excellent inhibition property of the corrosion in many metals in various aggressive media [10, 46]. It is understood that triazole ring adsorbs on the metal surface strongly in chloride solution making the formation of a complex with, metal and inhibits metal (copper or iron) corrosion possible by avoiding the creation of CuCl_2^- or FeCl_2^- by which metal dissolution happens.

3.8. SEM measurements

The scanning electron microscope images were recorded in order to confirm the creation of the films on the iron surface and establish the interaction of inhibitor molecule with the metal surface. In Figure 8a, SEM image of the surface bare metal sheet is indicated after polishing. In Figure 9 (b, c), SEM micrograph of C-steel is shown immersed for 1 hour in 1 mol L⁻¹ HCl without (Fig. 9b) and with 1 mol L⁻¹ of PDPTT (Fig. 9c). The morphology in Figure 9c shows a rough surface, characteristic of the uniform corrosion of C-steel in acid. A smooth surface can be seen with the PDPTT, displaying that the surface was protected by the inhibitor.

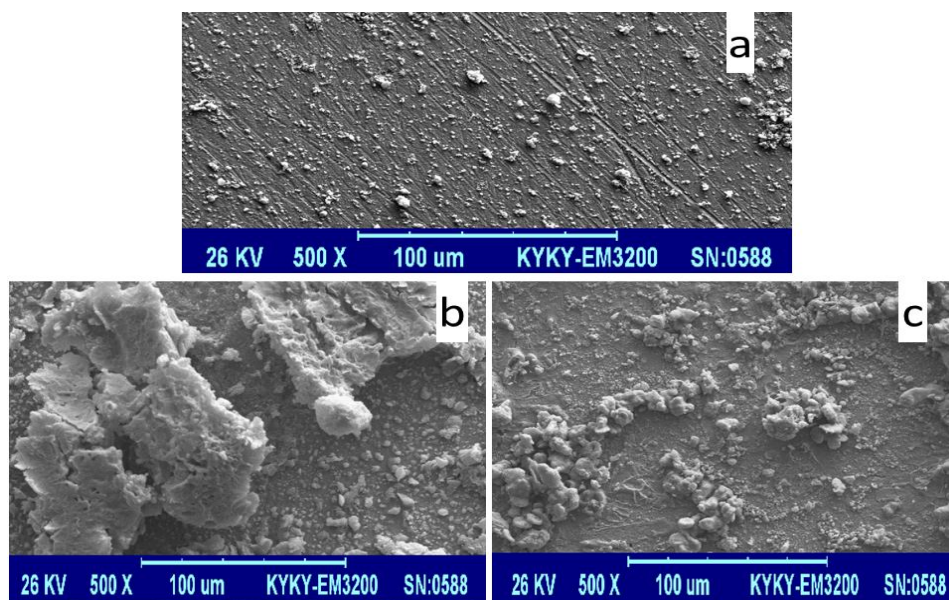


Figure 9. Scanning electron microscopy of mild steel samples (a) bare metal sheet after polishing (b) without inhibitor (Blank) and (c) containing 0.004 mol L⁻¹ of PDPTT.

4. CONCLUSION

(1) With an increase of the inhibitor concentration in acidic media inhibition is protected strongly.

(2) It is understood that the adsorption of PDPTT follows the Langmuir's adsorption isotherm through which the inhibition process occurs. The obtained $\Delta G_{\text{ads}}^{\circ}$ values reveal that the corrosion inhibition PDPTT is due to between chemi- and physisorption.

(3) Results of polarization studies suggest that the studied inhibitor behave as mixed type one.

(4) DFT method quantum chemical computations of parameters are related with the electronic structure. The values of quantum chemical parameters such as E_{HOMO} , E_{LUMO} and ΔN confirmed the PDPTT as an inhibitor with high performance.

(5) The obtained Inhibition efficiency decreased with increasing temperature and the values of the activation corrosion energy, standard enthalpy of activation and standard entropy of activation along with inhibitors increased with increasing temperature.

(6) The reactive sites predicted by condensed Fukui functions during electrophilic and nucleophilic are successfully produced once more.

(7) The SEM analysis showed that the metal surface was protected along with the PDPTT.

References

1. R. A. Prabhu, T. V. Venkatesha, A. V. Shanbhag, B. M. Praveen, G. M. Kulkarni, and R. G. Kalkhambkar, *mater. Chem. Phys.* 108 (2008) 283.
2. R. Solmaz, E. Altunbaş, and G. Kardaş, *mater. Chem. Phys.* 125 (2011) 796.
3. F. Bentiss, F. Gassama, D. Barbry, L. Gengembre, H. Vezin, M. Lagrenée, and M. Traisnel, *Appl. Surf. Sci.* 252 (2006) 2684.
4. H.-L. Wang, R.-B. Liu, and J. Xin, *Corros. sci.* 46 (2004) 2455.
5. F. Bentiss, B. Mernari, M. Traisnel, H. Vezin, and M. Lagrenée, *Corros. sci.* 53 (2011) 487.
6. M. Behpour, S. M. Ghoreishi, N. Mohammadi, N. Soltani, and M. Salavati-Niasari, *Corros. sci.* 52 (2010) 4046.
7. S.A. Abd El-Maksouda, A.S. Foudab, *Mater. Chem. Phys.* 93 (2005) 84.
8. E. El Ashry, A. El Nemr, and S. Ragab, *J. Mol. Model.* 18 (2012) 1173.
9. A. A. Abd-Elaal, I. Aiad, S. M. Shaban, S. M. Tawfik and A. Sayed, *J. Surfact. Deterg.* 17 (2014) 483.
10. E. M. Sherif and S.-M. Park, *Corros. sci.* 48 (2006) 4065.
11. M. K. Awad, M. R. Mustafa, and M. M. A. Elnga, *Journal of Molecular Structure: THEOCHEM* 959 (2010) 66.
12. Y. Kara, S. Sagdinc, and A. Esme, *Prot. Met. Phys. Chem. Surf.* 48 (2012) 710.
13. N. Foroughifar, A. Mobinikhaledi, and A. Rafiee, *J. Chem. Res.* 38 (2014) 111.
14. A. M. Abdel-Gaber, M. S. Masoud, E. A. Khalil, and E. E. Shehata, *Corros. sci.* 51 (2009) 3021.
15. I. B. Obot, N. O. Obi-Egbedi, and S. A. Umoren, *Corros. sci.* 51 (2009) 1868.
16. C. Lee, W. Yang, and R. G. Parr, *Phys. Rev. B: Condens. Matter* 37 (1988) 785.
17. M. J. Frisch et al. GAUSSIAN 03, Revision B.05, Gaussian, Inc., Wallingford, CT, 2004.
18. V. S. Sastri and J. R. Perumareddi, *Corrosion* 53 (1997) 617.
19. A. Popova, E. Sokolova, S. Raicheva, and M. Christov, *Corros. sci.* 45 (2003) 33.
20. F. Bentiss, M. Bouanis, B. Mernari, M. Traisnel, H. Vezin, and M. Lagrenée, *Appl. Surf. Sci.* 253 (2007) 3696.
21. S. K. Shukla, A. K. Singh, I. Ahamad, and M. A. Quraishi, *Mater. Lett.* 63 (2009) 819.
22. M. A. Deyab, *Corros. sci.* 49 (2007) 2315.
23. M. A. Hegazy, H. M. Ahmed, and A. S. El-Tabei, *Corros. sci.* 53 (2011) 671.
24. I. Ahamad, R. Prasad, and M. A. Quraishi, *Corros. sci.* 52 (2010) 3033.
25. R. Solmaz, *Corros. sci.* 52 (2010) 3321.
26. E. McCafferty and N. Hackerman, *J. Electrochem. Soc.* 119 (1972) 146.
27. L. Larabi, Y. Harek, M. Traisnel, and A. Mansri, *J. Appl. Electrochem.* 34 (2004) 833.
28. X. Li, S. Deng, and H. Fu, *Corros. sci.* 52 (2010) 2786.
29. R. Solmaz, G. Kardaş, M. Çulha, B. Yazıcı, and M. Erbil, *Electrochim. Acta* 53 (2008) 5941.
30. A. M. Atta, O. E. El-Azabawy, H. S. Ismail, and M. A. Hegazy, *Corros. sci.* 53 (2011) 1680.
31. D. A. López, S. N. Simison, and S. R. de Sánchez, *Electrochim. Acta* 48 (2003) 845.
32. M. Behpour, S. M. Ghoreishi, N. Soltani, M. Salavati-Niasari, M. Hamadani, and A. Gandomi, *Corros. sci.* 50 (2008) 2172.

33. M. A. Hegazy, A. S. El-Tabei, and H. M. Ahmed, *Corros. sci.* 64 (2012) 115.
34. A. K. Singh and M. A. Quraishi, *Corros. sci.* 52 (2010) 152.
35. V. S. Reznik, V. D. Akamsin, Y. P. Khodyrev, R. M. Galiakberov, Y. Y. Efremov, and L. Tiwari, *Corros. sci.* 50 (2008) 392.
36. R. Agrawal and T. K. G. Namboodhiri, *Corros. sci.* 30 (1990) 37.
37. A. Ostovari, S. M. Hoseinie, M. Peikari, S. R. Shadizadeh, and S. J. Hashemi, *Corros. sci.* 51 (2009) 1935.
38. F. Bentiss, M. Lebrini, and M. Lagrenée, *Corros. sci.* 47 (2005) 2915.
39. M. Bouklah, B. Hammouti, M. Lagrenée, and F. Bentiss, *Corros. sci.* 48 (2006) 2831.
40. D. K. Yadav, B. Maiti, and M. A. Quraishi, *Corros. sci.* 52 (2010) 3586.
41. S. Martinez and I. Stern, *Appl. Surf. Sci.* 199 (2002) 83.
42. M. J. S. Dewar, E. G. Zoebisch, E. F. Healy, and J. J. P. Stewart, *J. Am. Chem. Soc.* 107 (1985) 3902.
43. R. G. Parr and W. Yang, *J. Am. Chem. Soc.* 106 (1984) 4049.
44. F. De Proft, J. M. L. Martin, and P. Geerlings, *Chem. Phys. Lett.* 256 (1996) 400.
45. W. Yang and W. J. Mortier, *J. Am. Chem. Soc.* 108 (1986) 5708.
46. M. M. Antonijevic and M. B. Petrovic *Int. J. Electrochem. Sci.*, 3 (2008) 1.

© 2015 The Authors. Published by ESG (www.electrochemsci.org). This article is an open access article distributed under the terms and conditions of the Creative Commons Attribution license (<http://creativecommons.org/licenses/by/4.0/>).